# Influence of epoch time selection on the results of superposed epoch analysis using ACE and MPA data

Raluca Ilie,[1] Michael W. Liemohn,[1] Michelle F. Thomsen,[2] Joseph E. Borovsky,[2] and Jichun Zhang[3]

Received 31 March 2008; revised 5 September 2008; accepted 19 September 2008; published 17 December 2008.

[1] The influence of the reference time selection when conducting a superposed epoch analysis is examined for intense geomagnetic storms at solar maximum. The events were selected according to the minimum pressure-corrected *Dst*, *Dst**, being less than −100 nT. Solar wind data from ACE are used, along with near-Earth data from the magnetospheric plasma analyzer (MPA) instruments on the Los Alamos National Laboratory–operated geosynchronous spacecraft. Numerous choices for the zero epoch time are used, ranging from the storm sudden commencement (SSC), the peak of the ring current enhancement (minimum *Dst** slope), to the time of the storm peak (minimum *Dst** value). When doing superposed epoch analysis (SEA), the choice of the time stamp can be very important; for different choices, different storm characteristics are evident in the averaged data. In the superposed ACE data we find that when using the SSC as a time reference, the SSC-related jump in solar wind parameters is very well defined, but near the storm peak, $B_z$ does not apparently follow the well-known criteria for intense storms ($B_z \leq -10$ nT for more than 3 h), even though this criterion is met by most of the individual storms selected for this study. When the zero epoch time is chosen near the storm peak, the jump in solar wind parameters is less distinct (and eventually lost), but the criterion for $B_z$ is met. Regarding the MPA data, there are certain parameters that require the choice of a specific epoch time in order to produce a systematic behavior in the SEA analysis and others that are less sensitive to this choice of epoch time, since they appear to be less distinct in their temporal and spatial location. For instance, the nightside and morningside hot-ion density and temperature are main phase traits, and a zero epoch time near the peak of the ring current enhancement is required to make these features distinct.

**Citation:** Ilie, R., M. W. Liemohn, M. F. Thomsen, J. E. Borovsky, and J. Zhang (2008), Influence of epoch time selection on the results of superposed epoch analysis using ACE and MPA data, *J. Geophys. Res.*, *113*, A00A14, doi:10.1029/2008JA013241.

## 1. Introduction

[2] Magnetic storms and their solar wind drivers have been extensively investigated throughout the years. Because of the great amount of data available in recent years, a large variety of studies of these space weather events were performed in order to relate solar wind features to the corresponding geomagnetic responses [e.g., *Gonzalez and Tsurutani*, 1987; *Gonzalez et al.*, 1994; *O'Brien and McPherron*, 2000; *Huttunen and Koskinen*, 2004; *Zhang et al.*, 2006a]. Plasma observations at geosynchronous orbit are extremely advantageous for the study of storms and, in particular, for studying ring current sources since at this location the transition from plasma sheet to ring current is observed to take place [*Denton et al.*, 2005, 2006].

[3] The plasma sheet is the source of high-energy plasma injected into the inner magnetosphere by strong magnetospheric convection during magnetic substorms and storms, considered responsible for the ring current enhancement during times of high geomagnetic activity. Plasma sheet density has a direct influence on the strength of the ring current [e.g., *Thomsen et al.*, 1998; *Kozyra et al.*, 1998]. During the main phase of the storm, the plasma sheet can have access to geosynchronous orbit and to the inner magnetosphere [*Friedel et al.*, 2001; *Denton et al.*, 2005]. Statistical studies of the plasma at geosynchronous orbit showed that there is a correlation between plasma access and the *Kp* index [*Korth et al.*, 1999; *Thomsen*, 2004], and it varies with local time and particle energy. *Denton et al.* [2005] performed a superposed epoch analysis of storms in order to correlate the storm phase with the temporal variation of plasma found at geosynchronous orbit and showed that the solar cycle is one of the main controlling factors for the plasma sheet density. Moreover, the ion composition is found to be dependent on the solar cycle [*Young et al.*,

[1]Department of Atmospheric, Oceanic and Space Sciences, University of Michigan, Ann Arbor, Michigan, USA.
[2]Los Alamos National Laboratory, Los Alamos, New Mexico, USA.
[3]Physics and Astronomy Department, Rice University, Houston, Texas, USA.


0148-0227/08/2008JA013241

1982] and plasma properties at geosynchronous orbit have been shown to be well correlated with solar wind plasma properties [*Borovsky et al.*, 1998].

[4] The tool of superposed epoch analysis was previously used to investigate these complex magnetospheric disturbances, by categorizing the events according to several different characteristics. *Zhang et al.* [2006a, 2006b] and *Liemohn et al.* [2008] examined the features of magnetic storms relative to their intensity and time of occurrence (intense versus moderate versus superstorms, solar maximum versus solar minimum). Distinguishing the events by their solar wind drivers (e.g., CME versus CIR-driven storms) is another way to categorize them [*Pulkkinen et al.*, 2007; *Denton et al.*, 2006; *Borovsky and Denton*, 2006; *Huttunen et al.*, 2006; *Zhang et al.*, 2007]. It has been shown that corotating interaction regions (CIRs) and interplanetary coronal mass ejections (ICMEs) are the biggest contributors to magnetic disturbances at Earth [*Gosling et al.*, 1991; *Tsurutani and Gonzalez*, 1997]. *Feynman* [1980] found that CIRs predominately disturb *Kp* but not *Dst*, unlike CMEs, which perturb both *Kp* and *Dst*. *Denton et al.* [2006] showed that geosynchronous plasma responds differently during CME-driven storms than during CIR events; that is, during CME events, the plasma sheet density is one of the parameters that is preferentially enhanced, while CIR-driven storms produce an enhancement in the plasma sheet temperature.

[5] Most of the time, for statistical studies, the natural choice of the epoch time seems to be the peak storm intensity [*Zhang et al.*, 2006a, 2006b; *Liemohn et al.*, 2008; *Denton et al.*, 2005, 2006]. *Pulkkinen et al.* [2007] used the storm onset along with the minimum *Dst* as the epoch time when studying the differences between distinct drivers for magnetic storms, showing that the sheath storms develop faster at the storm onset and the main phase is shorter than in the case of cloud driven events. The storm sudden commencement was used as the epoch time by *Elphic et al.* [1996] as well, to look at the behavior of cold ions at geosynchronous orbit.

[6] It has been acknowledged that in order to describe the temporal variation of certain parameters, the choice of the time stamp might be important, but so far, there has been no systematic examination of the influence of this choice. In this paper we investigate how the choice of epoch time affects the average behavior of the storm time solar wind and geosynchronous plasma when doing superposed epoch analysis. For this study we selected seven distinct time stamps somewhat evenly distributed throughout the duration of the storm main phase.

## 2. Methodology

### 2.1. Data Coverage

[7] Solar wind IMF and plasma in situ observations are obtained from the ACE spacecraft in orbit around the L1 Lagrange point 1.5 million km upstream of the Earth. The data set, obtained from the National Space Science Data Center, consists of 4-min interplanetary magnetic field (IMF) data (from the MAG instrument) and 64-s solar wind plasma parameters (from the SWEPAM instrument). The plasma data were then averaged to 4 min temporal resolution, taking any 64 s value whose start minute fell between the start minute of the IMF data and 4 min later. The observations are converted from the GSE to GSM coordinate system and time propagated from the satellite location to (17Re, 0, 0), using the minimum variance analysis technique [*Weimer et al.*, 2003; *Weimer*, 2004]. Along with the ACE data, the 1 h resolution *Dst* index, provided by the World Data Center at Kyoto University, is used to study the geomagnetic responses to solar wind conditions.

[8] For the second half of this work, data are obtained from the magnetospheric plasma analyzers (MPA) on seven Los Alamos National Laboratory (LANL) geosynchronous satellites, which provide good local time coverage for most of the events. Each MPA instrument is a spherical sector electrostatic analyzer capable of measuring three-dimensional distributions of ions and electrons from ~1 eV to ~45 keV, on time scales of ~86 s. A detailed description of the instrument is given by *Bame et al.* [1993] and *McComas et al.* [1993]. The present study extends the work of *Zhang et al.* [2006a, 2006b]. The hot-ion fluxes ranging from 100 eV to 45 keV are used for the moments calculations, and since the MPA measurements do not contain any composition information for the positively charged particles, the calculation of the moments assumes that all ions are protons. For most conditions, this assumption is reasonable to within a factor of ~2 since *Young et al.* [1982] showed that, for energies below 17 keV at the geosynchronous orbit, $n_{O+}/n_{H+}$ is rarely greater than unity. However, during storm times the contribution of $O^+$ is known to increase substantially. In the case of $n_{O+}/n_{H+} \gg 1$ the plasma density would be four times higher than would be calculated under the assumption that $n_{O+}/n_{H+} \ll 1$ [*Liemohn et al.*, 1999]. Also, because of the fact that MPA measures energy per charge, the temperature measurements are not biased by the all-proton assumption. In the present paper we study the average nature of three derived bulk hot-ion parameters: number density ($N_{HP}$), total temperature ($T_{HP} = (T_{\|} + 2T_{\perp})/3$) and entropy density ($S_{HP} = T_{HP}/N_{HP}^{\gamma-1}$, where the polytropic index $\gamma = \frac{5}{3}$). To ensure that the measurements are taken in the plasma sheet, a limitation is set on the data such that $0.3\ \mathrm{cm}^{-3} < N_{HP} < 6\ \mathrm{cm}^{-3}$ and $T_{HP,\perp} > 2$ keV, excluding any measurements from the magnetosheath, low-latitude boundary layer and magnetotail lobes [*Korth et al.*, 1999]. The superposed epoch analysis technique enables us to illustrate the dependence of these plasma sheet parameters on local time and epoch time.

### 2.2. Event Selection

[9] According to the monthly averages of sunspot numbers, for this study we selected intense storms during the last solar maximum, i.e., from July 1999 to June 2002 (see Table 1). The pressure-corrected *Dst* index (*Dst**) is used to identify the intense storm, choosing events for which *Dst** $\leq -100$ nT. The motivation for using (*Dst**) instead of the *Dst* index in defining the storms is that the former contains mainly the contribution of the ring current and other near-Earth currents, while the magnetopause current input is removed. To compute the *Dst** we use the formula of *O'Brien and McPherron* [2000]:

$$Dst^* = Dst - 7.26 \cdot \sqrt{P_{dyn}} + 11.0 \qquad (1)$$

**Table 1.** List of Events Used for This Study

| Year | Month | Day | Hour (UT) | Minimum *Dst** (nT) |
|---|---|---|---|---|
| 1999 | Sep | 22 | 2300 | −178.45 |
| 1999 | Oct | 22 | 0700 | −251.76 |
| 1999 | Nov | 13 | 2200 | −104.01 |
| 2000 | Jan | 23 | 0300 | −105.47 |
| 2000 | Feb | 12 | 1100 | −141.49 |
| 2000 | Apr | 7 | 0000 | −306.42 |
| 2000 | May | 24 | 0800 | −147.73 |
| 2000 | Aug | 12 | 0900 | −236.44 |
| 2000 | Sep | 17 | 2300 | −215.12 |
| 2000 | Oct | 5 | 1300 | −192.15 |
| 2000 | Oct | 14 | 1400 | −105.15 |
| 2000 | Oct | 29 | 0200 | −124.29 |
| 2000 | Nov | 6 | 2100 | −168.38 |
| 2000 | Nov | 29 | 1300 | −120.65 |
| 2001 | Mar | 20 | 1500 | −147.82 |
| 2001 | Mar | 31 | 0800 | −401.21 |
| 2001 | Apr | 11 | 2300 | −278.33 |
| 2001 | Apr | 18 | 0600 | −127.62 |
| 2001 | Apr | 22 | 1500 | −103.20 |
| 2001 | Aug | 17 | 2100 | −115.82 |
| 2001 | Oct | 1 | 0800 | −149.97 |
| 2001 | Oct | 3 | 1400 | −164.23 |
| 2001 | Oct | 21 | 2100 | −202.63 |
| 2001 | Oct | 28 | 1100 | −159.92 |
| 2001 | Nov | 1 | 1000 | −102.28 |
| 2002 | Mar | 24 | 0900 | −103.65 |
| 2002 | Apr | 20 | 0600 | −156.91 |
| 2002 | May | 11 | 1900 | −102.85 |
| 2002 | May | 23 | 1700 | −116.35 |

where $P_{dyn}$ is the solar wind dynamic pressure in nPa. Out of the 34 events that occurred during this period, only 29 were analyzed in this work; 5 storms were excluded because of lack of solar wind data.

### 2.3. Data Analysis Technique

[10] Superposed epoch analysis (SEA) is a statistical method that combines data from similar but distinct events by defining a reference time (also called epoch time, time stamp and time mark) within each event in order to be used as a mark in the computation of means for each parameter within the selected category. Time marks for each event are chosen in such a way so that $t = 0$ (the so-called epoch time) corresponds to some common feature in the superposed data. In the present study we choose seven distinct time references within the development of the storms, ranging from the storm sudden commencement (SSC) to the peak development of the storm (minimum *Dst*). The SSC was defined as the time corresponding to the maximum slope of *Dst* closest to the SSC, except for the cases when there is no obvious jump in solar wind pressure when the SSC time mark was manually chosen to correspond with the southward turning of the IMF $B_z$ component. The slope of the *Dst* index was defined as:

$$Dst\ slope\left(t_n + \frac{1}{2}\right) = Dst(t_{n+1}) - Dst(t_n) \tag{2}$$

such that the maximum value of the slope corresponds to an increase in the index itself while the minimum value of the slope coincides to the steepest decrease in *Dst*. We choose the slope of the *Dst* index as opposed to the slope of *Dst** to define our reference times mainly because *Dst* index includes the effect of the dynamic pressure change at the shock associated with SSC while the storm sudden commencement is removed from the *Dst** index. The peak enhancement of the ring current was defined as the minimum *Dst* slope (corresponding to the maximum negative slope). The minimum slope search was performed from the location of the maximum slope to the location of the minimum *Dst* (except 4 events for which it was manually chosen).

[11] Aside from the obvious choice of minimum *Dst* as a reference time and the ones mentioned above, four additional marks were chosen: $median_1$, $median_2$, $median_3$ and $median_4$ defined below:

$$median_1 = \frac{1}{2} \cdot (time\ of\ minimum\ Dst - time\ of\ minimum\ slope) + time\ of\ minimum\ slope \tag{3}$$

$$median_n = \frac{n-1}{4} \cdot (time\ of\ minimum\ slope - time\ of\ maximum\ slope) + time\ of\ maximum\ slope \tag{4}$$

for $n = 2, 3, 4$.

[12] To illustrate these choices, Figure 1 shows the dynamic pressure (first panel), $B_z$ component of the interplanetary magnetic field (second panel), the *Dst* index (black dotted line) along with the pressure corrected *Dst** (black continuous line) (third panel), and on the fourth panel the computed slope of the *Dst* index for the 17 April 2001 event. This storm is a typical example of the data set we are studying (but it has a short main phase), given that it shows a clear jump in solar wind dynamic pressure, followed by a southward turning of the IMF $B_z$, and the maximum slope of *Dst* corresponding to the storm sudden commencement.

[13] To be quantitative, we define the main phase as the time interval between the storm sudden commencement (maximum *Dst* slope) and the peak development of the storm corresponding to the minimum *Dst* index. Within the main phase we defined the early main phase as the time period starting at the SSC and ending at the location where the ring current has its maximum intensification (minimum slope of *Dst*). The late main phase is defined as the period of time that starts at the peak enhancement of the ring current and ceases where the recovery phase starts (when the *Dst* returns to its quiet time value).

[14] For this event, the main phase lasted for 5.5 h, the early main phase and the late main phase having durations of 3 and 2.5 h, respectively. The vertical dashed lines in Figure 1 show all the epoch choices for our study. The plots represent 12 h worth of data.

## 3. Results

### 3.1. Storm duration

[15] As an initial study for our work, we looked at the average duration of the main phase of the storms. Statistical analysis of these periods (Figure 2) of time yielded the following results: the average main phase duration of a

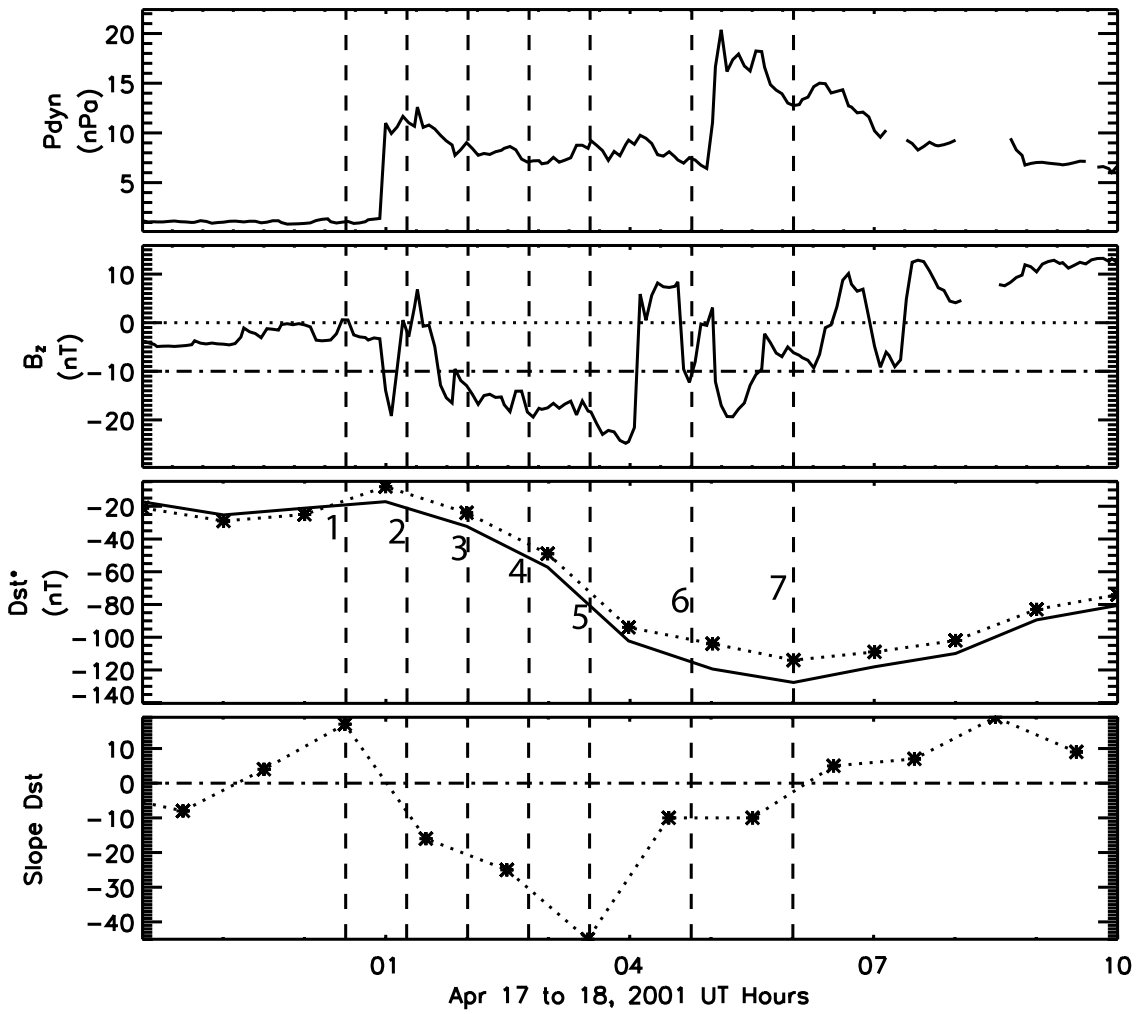


**Figure 1.** Event of 17 April 2001. The first panel plots the dynamic pressure ($P_{dyn}$), the second panel plots the $z$ component of the interplanetary magnetic field ($B_z$), the third panel plots the pressure-corrected *Dst* index (*Dst**) (continuous line) along with *Dst* index (the dotted line), and the fourth panel plots the slope of the *Dst* index. Vertical lines indicate the position of different epoch time choices: SSC, maximum slope of *Dst* index (line 1); $median_2$ (line 2); $median_3$ (line 3); $median_4$ (line 4); minimum slope of *Dst* index (line 5); $median_1$ (line 6); and minimum *Dst* (line 7). Symbols are added to show the slope and *Dst* data points.

storm is 13.2 h with a median (the 50th percentile) of 11.5 h while the average duration of the early main phase is 7.2 h with a median of 7 h. Also the average duration of the late main phase is 6 h with a median of 4 h.

[16] Three additional time stamps (equally spaced in time), during the early main phase and of just one during the late main phase were selected for our study. That is, for an average length storm, the 7 reference times are equally spaced about every 2 h throughout the main phase.

### 3.2. Solar Wind Data

[17] Superposed epoch means of selected parameters for the 29 storms at solar maximum are presented in Figure 3. Figures 3a and 3b show the superposed average values of solar wind dynamic pressure ($P_{dyn}$), Figures 3c and 3d present the $z$ component of the interplanetary magnetic field ($B_z$), and the Figures 3e and 3f show the pressure-corrected *Dst* index (*Dst**). The three differently colored lines correspond to the results obtained using distinct time stamps: the red line corresponds to maximum *Dst* slope, i.e., the SSC as the epoch time; the blue line corresponds to the minimum *Dst* slope; and the black line corresponds to minimum value of the *Dst* index. Figures 3a, 3c, and 3e show the means plotted against the time relative to the epoch time. The vertical dashed line corresponds to the location of the time stamp (zero epoch time). The plots show results for within 1.5 days before and after the epoch time. The horizontal dashed lines in the $B_z$ and *Dst** panels denote the 80% occurrence level thresholds for intense storms (for intense storms with a measured *Dst* less than or equal to $-100$ nT, 80% occur when the $z$ component of the interplanetary magnetic field is less or equal to $-10$ nT for a time interval of more than 3 h) as defined by *Gonzalez et al.* [1994] and *Gonzalez and Tsurutani* [1987]. When using maximum slope as the epoch time (red curves), the SSC-related jump in solar wind dynamic pressure is very well reproduced,

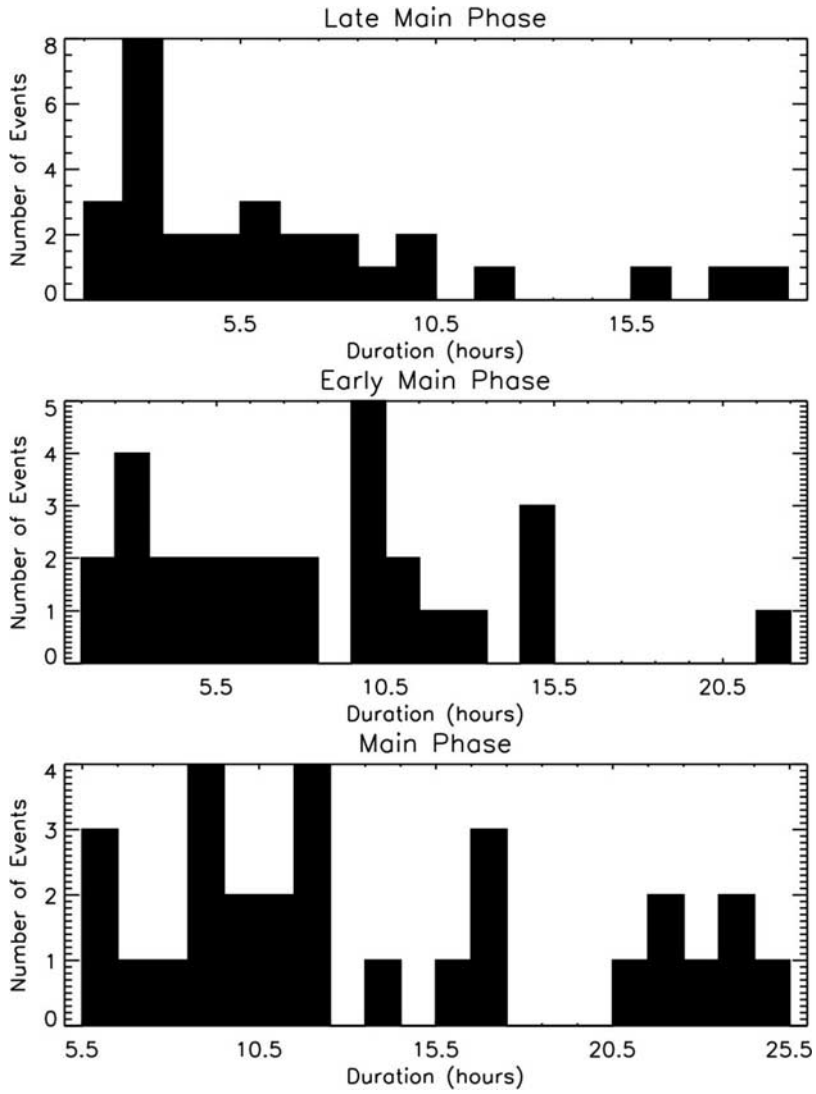


**Figure 2.** Histogram of the storm phase durations: (top) late main phase, (middle) early main phase, and (bottom) main phase.

with the pressure ramping up and jumping from about 2.25 nPa just before the 0 time to about 8.5 nPa just 1 h after. Near the storm peak, however, $B_z$ for this choice of the epoch time does not follow the well-known criterion for intense storms ($B_z \leq -10$ nT for more than 3 h), having values not lower than $-8$ nT. Note that most of the individual events used in this study were selected to follow this criteria. The averaged *Dst* shows a slow drop, taking about 12 h until it reaches the minimum value of approximately $-120$ nT.

[18] When the time stamp is set at the storm peak (black curves), the jump in solar wind dynamic pressure is less distinct (and eventually lost) with the solar wind dynamic pressure gradually increasing, but the standard criterion for $B_z$ is met. The averaged minimum *Dst* for this case is less than $-165$ nT and the *Dst* decreases rapidly prior to minimum.

[19] For the situation when the minimum slope of *Dst* is set as the time stamp (blue curves), the superposed means show $B_z \leq -10$ nT for more than 3 h, with a minimum value similar to the previous case. The jump in dynamic pressure is not sharp at all and we see that the superposed ram pressure peaks at the moment when the intensification of the ring current is maximum. This is due to the averaging of a few storms that happened to have a high pressure a few hours after the storm SSC. The *Dst* index shows again a sharp decrease, having a comparable slope as in the previous case, peaking at about $-140$ nT this time. Also, the $B_z$ in both situations has similar traits, reaching almost the same minimum value. We note that at the beginning of the storm, the *Dst* averaged relative to the peak of the storm descends at a slightly slower pace than the one averaged at the peak enhancement of the ring current, mainly because the $B_z$ turns southward in a more gradual manner than in the latter case when the gradient of $B_z$ is higher. Therefore, as previously shown, the controlling factor in the rate of change of *Dst* is the southward component of the IMF [e.g., *Burton et al.*, 1975]. In Figure 3e, the minimum averaged *Dst* occurs at different epoch times for different zero-epoch choices.

[20] Figures 3b, 3d, and 3f show the same mean values shifted relative to the location of the means when averaged

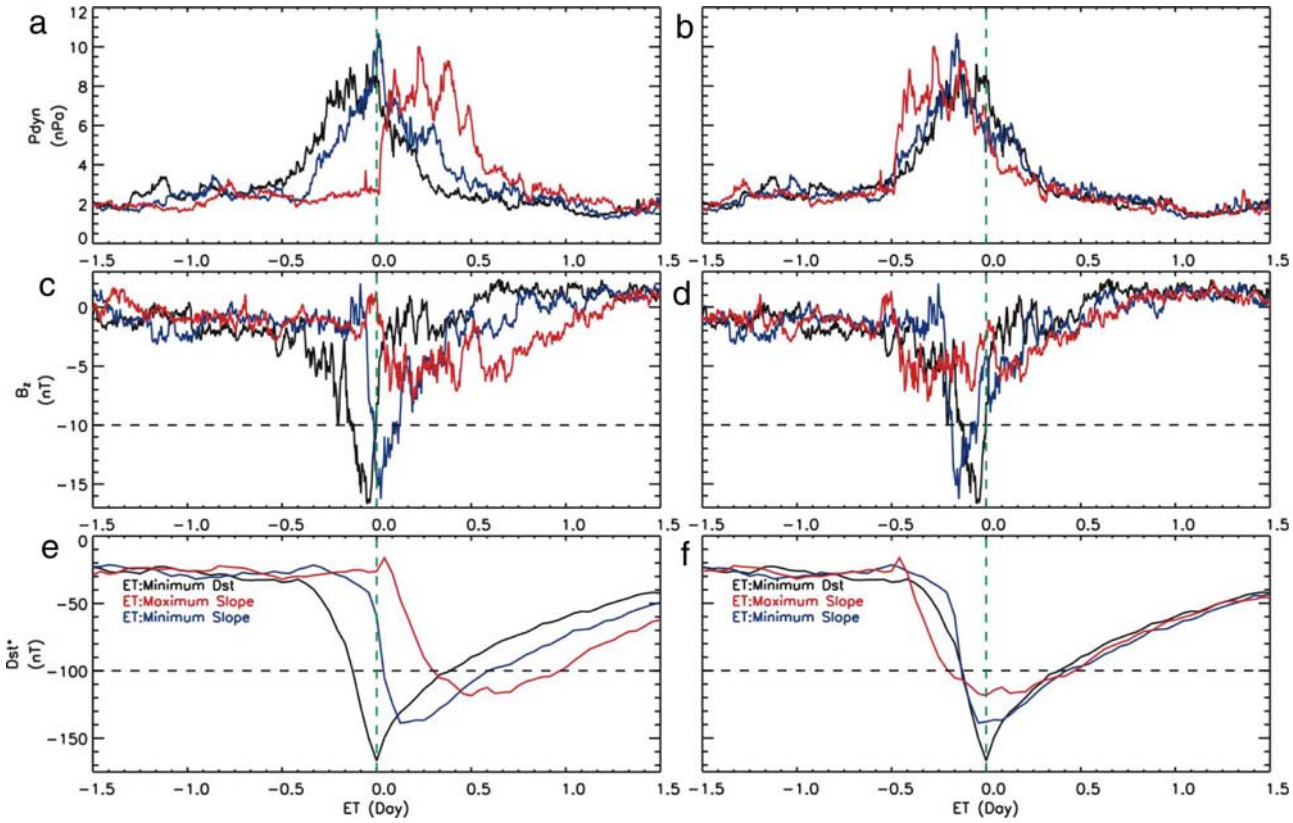


**Figure 3.** Superposed epoch means for 29 intense storms at solar maximum. (a and b) The superposed averaged values for the dynamic pressure ($P_{dyn}$), (c and d) the $z$ component of the interplanetary magnetic field ($B_z$), and (e and f) the pressure corrected *Dst* index (*Dst**) for three different choices of the time stamp: red line, maximum *Dst* slope; blue line, minimum *Dst* slope; and black line, minimum value of *Dst* index. Figures 3a, 3c, and 3e are plotted relative to the epoch time while Figures 3b, 3d, and 3f show the same mean values shifted relative to the location of means when averaged at the *Dst* minimum.

at the *Dst* minimum. The time shift of the blue and red lines relative to the black ones is 4 and 12 h, respectively. This is in good agreement with our findings regarding the duration of the main phase. Note that we only choose one zero-epoch time in our superposed epoch analysis, therefore the means are not normalized with respect to the duration of the storms. Consequently, it is expected that the minimum averaged *Dst* when superposing our data at the minimum *Dst* slope (maximum *Dst* slope) does not occur exactly 6 (13.2) h from the location of minimum averaged *Dst* when superposing at the minimum *Dst*. This is due to the fact that phase lengths of the individual storms are variable. Please note that the closer to the storm peak the epoch time is selected, the shorter the length of main phase gets with the late main phase following the $B_z$ ramp of the storm. Thus, by changing the epoch time in our analysis, not only the average intensity of the set changes but also certain features used to identify the events are no longer reproduced by the superposed data. The *Gonzalez et al.* [1994] criterion to produce an intense storm is met only if the superposition of the data is done in the interval between the $median_4$ (which is, on average, 6 h before the storm maximum and not shown in Figure 3) and storm peak.

### 3.3. MPA Data

[21] Figure 4 presents the superposed epoch analysis of geosynchronous plasma parameters for the 29 intense storms for just three choices of the epoch time (maximum *Dst* slope, minimum *Dst* slope and minimum *Dst*). For each choice of the epoch time, the hot-ion density ($N_{HP}$), temperature ($T_{HP}$) and entropy density ($S_{HP} = T_i/N^{2/3}$) [*Birn et al.*, 2006] values, as a function of universal time versus local time, are grouped into bins of 1 h temporal resolution and averaged essentially in the same manner as described by *Zhang et al.* [2006b]. The color scale is linear and showed only in Figures 4i–4l (as in the work by *Zhang et al.* [2006b]). Purple (black) bins correspond to values exceeding the maximum (minimum) value on the color scale. When the time stamp is set at the peak enhancement of the ring current (minimum slope of *Dst*, Figures 4e–4h), the density peaks around storm maximum and the entropy density shows a minimum a few hours into the recovery phase on the dayside. When the epoch time is chosen at the beginning of the storm (maximum slope of *Dst*, Figures 4a–4d), the density at the storm peak is not as high as for the case when the time stamp is set at the peak of the storm (minimum *Dst*, Figures 4i–4l). An interesting feature is that we see little to no variation in the temperature behavior for all three situations, with a temperature intensification in the afternoon sector in the early main phase of the storm and a minimum at the peak of the storms. We conclude that the late main phase of the storm has the highest concentration of

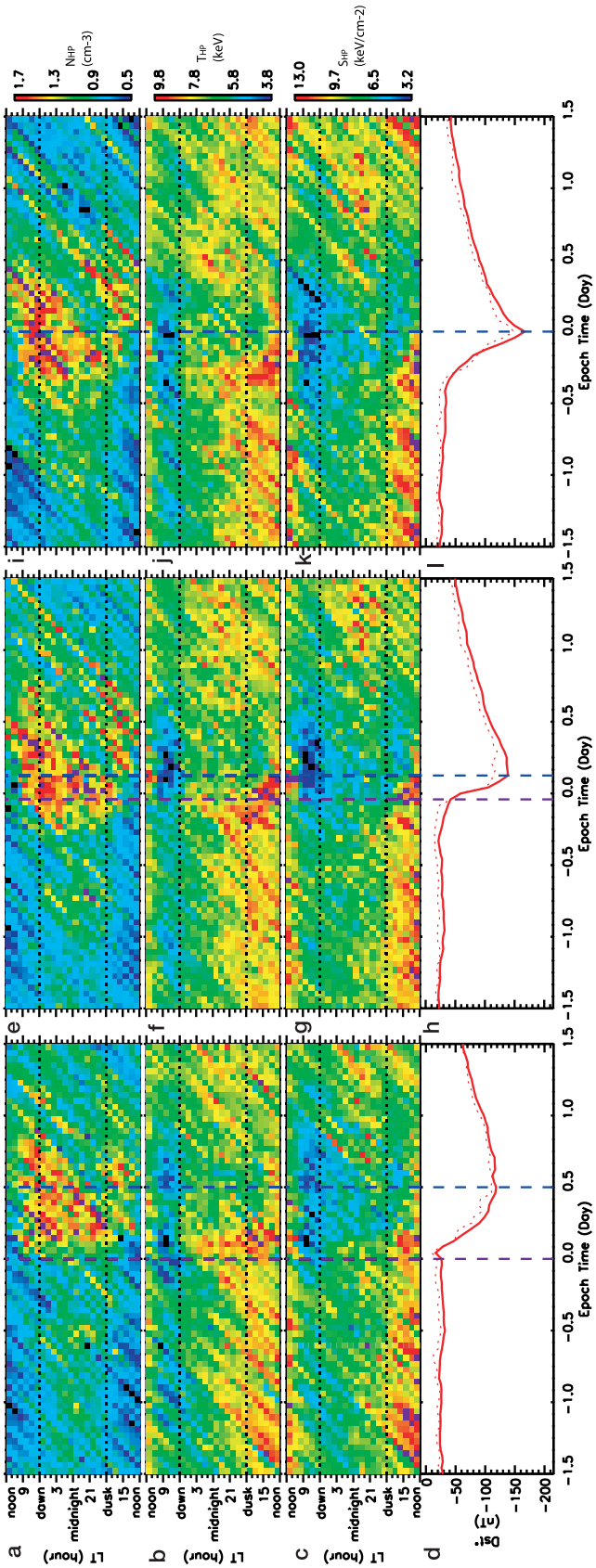


**Figure 4.** Superposed epoch data from the MPA instruments for three distinct epoch times. (a–d) Maximum slope of *Dst*, (e–h) minimum slope of *Dst*, and (i–l) the minimum *Dst*. Shown are the hot proton density ($cm^{-3}$) (Figures 4a, 4e, and 4i), the hot proton temperature (keV) (Figures 4b, 4f, and 4j), the entropy density (keV $cm^{-2}$) (Figures 4c, 4g, and 4k), and the *Dst* (dotted line) and *Dst** (continuous line) indices (nT) (Figures 4d, 4h, and 4l). The purple dashed vertical line in all plots shows the location of the 0 time while the blue dashed vertical line represents the location of the minimum superposed *Dst* time mark.

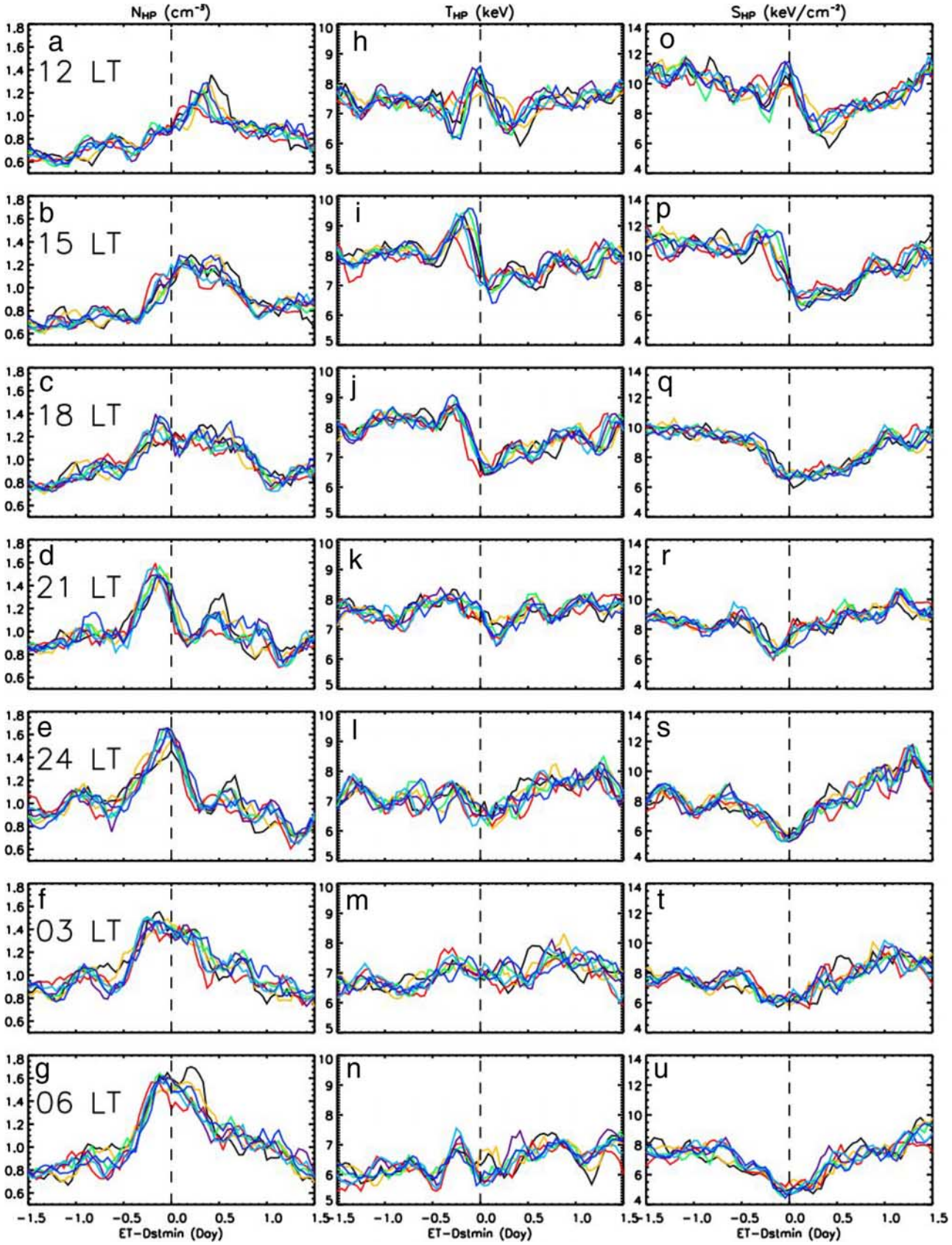
N_HP (cm^-3)
T_HP (keV)
S_HP (keV/cm^-2)
a
12 LT
b
15 LT
c
18 LT
d
21 LT
e
24 LT
f
03 LT
g
06 LT
h
i
j
k
l
m
n
o
p
q
r
s
t
u
ET-Dstmin (Day)
ET-Dstmin (Day)
ET-Dstmin (Day)

**Figure 5**

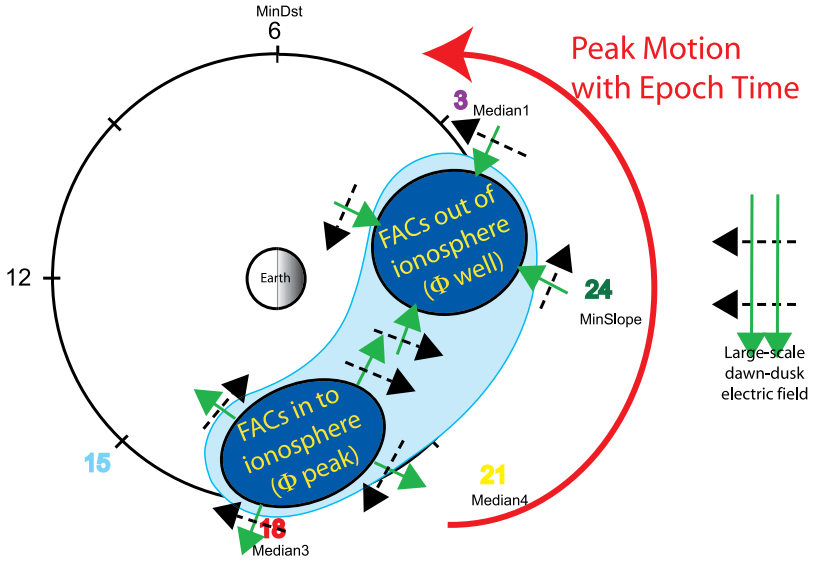


**Figure 6.** Illustration of the motion of density peak during the development of the storm. The view is in the equatorial plane of the Earth, looking down from over the North Pole. The green arrows show the dawn to dusk convection electric fields, and the dashed arrows show the $E \times B$ drift. The regions of the field aligned currents (FAC) are denoted by the black sectors. The "Φ peak" and "Φ well" refer to the potential peak and well that form when plasma from the magnetotail moves toward the inner magnetosphere. The labels median 1–4, MinSlope, and MinDst at various LTs show the location of the peak when the averaging is done using these epoch times.

particles, when the ring current is at its peak, while the early main phase is dominated by temperature enhancements.

[22] If no losses to the plasma occurred, then adiabatic convection from the nightside to the dayside during a storm would produce a density increase and a temperature increase with the specific entropy density being constant. As can be seen in Figures 4c, 4g, and 4k, before the storm and during the early phase of the storm the entropy density increases from midnight to noon. This is as expected for the flow of the hot ions from the nightside to the dayside through the hydrogen geocorona, where charge exchange loss creates an ion distribution that is hotter and less dense on the dayside. As can be seen in Figure 4c, during the storm main phase the entropy density increase from the nightside to the dayside is even larger, and the density decrease from the nightside to the dayside is even larger. This may be an indication of pitch-angle-scattering loss of ions to the atmosphere in addition to charge exchange losses during the storm main phase. During the recovery phase (Figure 4k) the density, temperature, and entropy density trends from the nightside to the dayside are not consistent with adiabatic convection plus charge exchange. In particular, the entropy density is lower on the dayside than it is on the nightside. Future work using computer simulation is needed to determine what produces this entropy density gradient.

[23] The entropy density increases from midnight to the dayside, and the low entropy density in the morning region is a feature seen in all three cases, but the transient, very low entropy density, morning features are captured only when the superposition is done close to the peak of the storm.

[24] To quantitatively investigate these results, Figure 5 presents line plots of the average hot-ion density ($N_{HP}$), temperature ($T_{HP}$) and entropy density ($S_{HP}$) for each of the epoch times used in this study. These values were extracted from Figure 4 at seven local times. Again, the mean values for all parameters are shifted relative to the location of means when averaged at the *Dst* minimum. In order to reduce the statistical error in our bins, we have smoothed the data for all the MPA line plots by performing running averages with a window of 5 h. We see that at different local times, the densities peak at different times during the storm, i.e., at different epoch times, and therefore we observe a motion of the particle peak density from the afternoon sector toward the morningside as the storm progresses. This progression might seem counterintuitive given the fact that ions drift in the opposite direction. *Liemohn and Brandt* [2005] provide a possible scenario to explain this motion (Figure 6): When the hot plasma is moved into the inner magnetosphere, the ion drift around the pressure peaks alters the local flow of material. Subsequent injections generate new vortices and the flow is diverted eastward.

**Figure 5.** Superposed epoch data from the MPA instruments showing epoch time profiles extracted from the results in Figure 4. (a–g) The hot proton density ($cm^{-3}$), (h–n) the hot proton temperature (keV), and (o–u) the entropy density (keV $cm^{-2}$) for different choices of epoch time. Each row corresponds to a certain local time while the color lines represent the distinct time marks: maximum slope of *Dst* (blue), $median_2$ (light blue), minimum slope of *Dst* (red), $median_1$ (yellow), $median_4$ (green), $median_3$ (purple), and minimum *Dst* index (black).

This motion accounts for the spatially varying inflow of fresh particles from the plasma sheet.

[25] The averaged temperature, seen in Figures 5h–5n, shows strong temporal variations only in the afternoon sector, with the noon hot-ion temperature having the maximum value at the peak development of the storm while the 1500 LT and 1800 LT temperatures peak just before the storm maximum. This dayside peak in temperature, seen only with an epoch time early in the main phase of the storm, is an observation of the loss of the prestorm hot ions out of the inner magnetosphere as they are convected out past geosynchronous orbit. In all the other local times, the temperature is relatively constant. The peak otherwise is lost when the averaging is done using a time stamp later in the storm development. Therefore the flow of the preexisting ring current is seen best with early epoch time choices.

[26] The superposed entropy density, seen in Figures 5o–5u, shows minimum values at the epoch time in the afternoon and night sector. The noon and 1500 LT entropy density shows some variation with the noon entropy density peaking at the zero-epoch time. This is to be expected since the entropy density is a derived parameter, therefore its behavior is determined by that of density and temperature.

[27] Figure 7 shows a presentation similar to that of Figure 5, except that each row corresponds to a different zero epoch, and the colored curves correspond to different local times. The 0600 LT density peaks at the peak of the storm with a maximum value of 1.65 $cm^{-3}$, the 0300 LT density peaks at $median_1$ with a maximum value of 1.49 $cm^{-3}$, midnight density peaks somewhere around the minimum *Dst* slope with a maximum value of 1.4 $cm^{-3}$, the 2100 LT peaks at $median_4$ with a maximum value of 1.64 $cm^{-3}$, the dusk density peaks close to the start of the storm with a maximum value of 1.2 $cm^{-3}$, while the dayside local time densities peak sometime during the recovery phase of the storm. The 1200 LT and 1500 LT densities are the lowest, independent of the epoch time choice, while the density at dawn shows the highest values. Also, independent of the time stamp, the 0600 LT temperature has the lowest values, while the 1800 LT and 1500 LT hot proton temperatures have the highest values in all seven cases. These findings are in good agreement with *Denton et al.* [2005], who showed that the hot proton density is mostly enhanced on the dawnside and duskside, while the temperature on the dawnside is lower than the temperature on the duskside.

[28] We notice a westward enhancement of the densities, starting with high values at dawn and decreasing peak densities westward through the nightside. This corresponds to an enhancement of the proton density in the morning sector. The nightside temperature (midnight, 2100 LT, 0300 LT, 0600 LT) shows little to no variation while the dayside hot-ion temperature has maximum values during the main phase of the storm, followed by a drop of about 20% of its value at the peak of the storm. Similarly to the temperature, the entropy density has minimum and maximum values on the dayside and almost no variation on the nightside. The average drop in the entropy density is of approximately 17%. This is in agreement with the findings for density and temperature.

[29] In order to quantify the effects of choosing different reference times when doing superposed epoch analysis, it is useful to perform a statistical test on some of the moments values from the different epoch time results. Figure 5 is particularly useful for this, in which the averaged moments from the different reference time choices are directly compared. It can be seen that there are certain times and places within the plots of Figure 5 when there is a large amount of spread between the moments values. It is these places that will be systematically considered to identify when the reference time choice is important.

[30] Specifically we conducted significance tests for some of the maximum and minimum values within Figure 5. For the hot-ion density column, the maximum value within the plot was compared against the minimum value at the same epoch time. That is, a vertical line was drawn straight down from the peak value within any one density panel, and the peak value was compared against the minimum value along that vertical line, from whichever other reference time result is the lowest there. So, for example, for the hot-ion densities at 1200 LT (Figure 5a), the peak value is from the curve for the minimum *Dst* reference time (black curve, $\sim$1.35 $cm^{-3}$ at ET = 0.4 days), which was compared with the corresponding value from the minimum slope reference time at ET = 0.4 days (red curve, $\sim$0.95 $cm^{-3}$). For the hot-ion temperature results in Figure 5, again the peak temperature value was found and compared with the minimum temperature at the same epoch time, from whichever reference time result is lowest at that place in the plot. For the entropy density results, the procedure is reversed: the minimum value of each plot was compared with the maximum value at the same epoch time.

[31] Using these values, the Student $t$ test statistics and significance were calculated for the hot-ion density, temperature and entropy density means using all seven choices of epoch times. $t$ test statistics $T$ of two populations $x = (x_0, x_1, \ldots, x_{N-1})$ with mean $\bar{x}$ and $y = (y_0, y_1, \ldots, y_{M-1})$ with mean $\bar{y}$ is computed in the following way:

$$T = \frac{\bar{x} - \bar{y}}{\sqrt{\frac{\sum_{i=0}^{N-1}(x_i - \bar{x})^2 + \sum_{i=0}^{M-1}(y_i - \bar{y})^2}{N+M-2} \cdot \left(\frac{1}{N} + \frac{1}{M}\right)}} \tag{5}$$

i.e., the ratio of the means difference to the standard error of differences. The series elements are all of the real data that contributed to the average values for the two specific points from Figure 5 that are being compared. For example, for the hot-ion densities at 1200 LT (Figure 5a), the two points being compared (from the red and blue curves at ET = 0.4 days) contain 342 and 303 observations (which are summation ranges N and M in equation (5)).

**Figure 7.** Superposed epoch data from the MPA instruments showing local time profiles extracted from the results in Figure 4. (a–g) The hot proton density ($cm^{-3}$), (h–n) the hot proton temperature (keV), and (o–u) the entropy density (keV $cm^{-2}$) for different choices of epoch time. Each row corresponds to a certain epoch time while the color lines represent the distinct local times: noon (blue), 1500 LT (light blue), 1800 LT (red), 2100 LT (yellow), midnight (green), 0300 LT (purple), and 0600 LT (black).

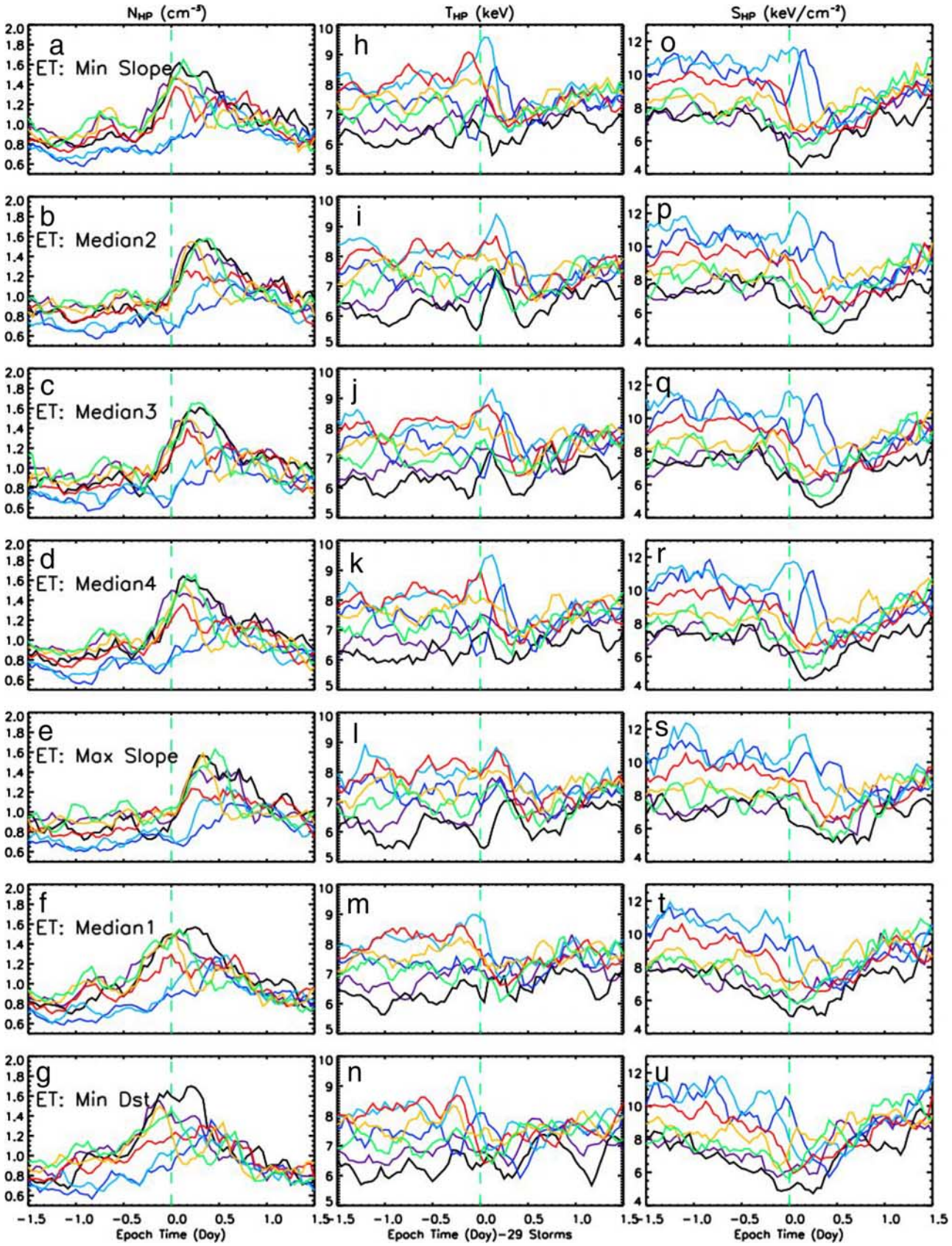
$N_{HP}$ (cm$^{-3}$)
$T_{HP}$ (keV)
$S_{HP}$ (keV/cm$^{-2}$)
a
ET: Min Slope
b
ET: Median2
c
ET: Median3
d
ET: Median4
e
ET: Max Slope
f
ET: Median1
g
ET: Min Dst
h
i
j
k
l
m
n
o
p
q
r
s
t
u
Epoch Time (Day)
Epoch Time (Day)−29 Storms
Epoch Time (Day)

**Figure 7**

**Table 2.** Significance Values for Hot-Ion Density, Temperature, and Entropy Density Correlations Between Data Points Contained by the Maximum and Minimum Values at the Corresponding Epoch Time[a]

| LT | $N_{MAX}$ | $T_{MAX}$ | $S_{MIN}$ |
|---|---|---|---|
| 1200 | **8.9** $\times 10^{-10}$ | **4.8** $\times 10^{-34}$ | **3.8** $\times 10^{-4}$ |
| 1500 | **5.0** $\times 10^{-2}$ | **1.7** $\times 10^{-11}$ | **2.6** $\times 10^{-44}$ |
| 1800 | **1.9** $\times 10^{-3}$ | **9.2** $\times 10^{-18}$ | 0.3 |
| 2100 | 0.1 | **4.2** $\times 10^{-2}$ | 0.3 |
| 2400 | **1.4** $\times 10^{-4}$ | **3.5** $\times 10^{-22}$ | **1.4** $\times 10^{-27}$ |
| 0300 | **7.2** $\times 10^{-6}$ | 0.5 | **1.9** $\times 10^{-9}$ |
| 0600 | **3.8** $\times 10^{-15}$ | **2.6** $\times 10^{-5}$ | 0.7 |

[a]Boldface numbers indicate values below the 5% correlation limit.

[32] The significance of the *t* test represents the probability that the two samples of populations have significantly different means. The significance is a value in the interval [0.0, 1.0], and a small value of less than 0.05 is indicative of the fact that *x* and *y* have significantly different means, while a value of 1.0 corresponds to 100% correlation between the samples.

[33] The *t* test statistics were calculated between the points that make up the maximum value of each averaged quantity and the points that account for the minimum value at the same universal time. The results are shown in Table 2. These statistics were calculated using the averaged quantities shown in Figure 5. Each of the numbers represents the significance value for different populations. We note that when superposing at maximum *Dst* slope, the peak in noon density is not as sharp as when we superpose the data at minimum *Dst* slope. When the epoch time is chosen close to the start of the storm ($median_2$), we note a peak in the noon temperature, a peak that is lost when the epoch time is set at close to the maximum intensification of the storm, meaning that the numbers that go into the peak value of temperature are significantly different than the ones that go into the averaging at the minimum *Dst* at the same epoch time. For the 2100 LT density and entropy density, 0600 LT entropy density and 0300 LT temperature, the maximum and the minimum values are not significantly different, meaning that most likely, they come from the same populations. For all the other local times, all parameters have significantly different means. Therefore, the choice of the epoch time matters primarily in accurately depicting the size of the peak in all of the averaged quantities. Qualitatively, the presence and shape of the peaks is unaltered by the time stamp used in the analysis.

## 4. Discussion and Conclusions

[34] We have reported on the importance of epoch time selection when doing statistical studies using the superposed epoch analysis. We have performed the averaging of 29 solar maximum intense storms using both solar wind data from ACE and geosynchronous observations by the MPA instruments from LANL satellites. The results presented above show clearly that certain parameters require a certain epoch time in order to reproduce an accurate behavior, and others are less sensitive to the epoch time choice when doing superposed epoch analysis, since they exhibit less spatial and temporal variation. The *Gonzalez et al.* [1994] convention commonly used to illustrate intense storm behavior is met by superposed storm profiles, only if the superposition of the data is done at the $median_4$ or later, i.e., no earlier than about 6 h before the storm peak for an average length storm. In addition, when the zero epoch time is set near the minimum *Dst* index, the storm sudden commencement features are lost.

[35] The average duration of the main phase is found to be 13.2 h. This result is somewhat in agreement with *Pulkkinen et al.* [2007], who found that the average duration of sheath storms is of about 8 h while the main phase in the case of cloud storms lasts for about 14 h. Note that in our study we do not differentiate between the storm drivers and we only study storms that occurred during the solar maximum. However, CME-driven storms occur with predilection during solar maximum [*Richardson et al.*, 2001], so our data set is probably dominated by such storms, thus our claim that our result for the main phase duration is in agreement with the findings of *Pulkkinen et al.* [2007] is justified. Moreover, the ring current takes about 7.2 h on average to reach maximum enhancement while the late main phase lasts for approximately 6 h, in agreement with her CME main phase duration findings of 14 h.

[36] We have investigated the characteristics and the temporal evolution of geosynchronous plasma parameters as a function of local and epoch time. Our results show an eastward motion of the particle peak density with different local time densities peaking at different moments during the development of the storm. These findings lead us to conclude that this motion describes the inflow of fresh plasma sheet particles into the inner magnetosphere. Conversely, flow-out of the preexisting ring current is seen best with early epoch times. Thus the noon temperature is one of the bulk ion parameters that requires a time stamp closer to the start of the storm in order to be resolved in the averaging.

[37] Furthermore, our findings indicate that a distinct epoch time is needed to accurately resolve certain solar wind features; when looking at the hot protons at geosynchronous orbit, the choice of the epoch time primarily matters in accurately depicting the size of the peak in all averaged quantities while the presence and shape of the peaks is unaltered by the time stamp used in the analysis.

[38] **Acknowledgments.** The Michigan authors would like to thank NASA and NSF for supporting this research (specifically, grants NNG05GE02G, NNG05GM48G, NNG05GJ89G, and ATM-0203163) and also LANL IGPP for additional support of the graduate student involvement in this study. The authors would like to thank the National Space Science Data Center for providing the ACE data: MAG instrument (N. F. Ness) and SWEPAM instrument (D. McComas). Work at Los Alamos was performed under the auspices of the U.S. Department of Energy, with partial support from the NASA LWS program.

[39] Wolfgang Baumjohann thanks Ian Richardson and another reviewer for their assistance in evaluating this paper.

## References

Bame, S. J., B. E. Goldstein, J. T. Gosling, J. W. Harvey, D. J. McComas, M. Neugebauer, and J. L. Phillips (1993), Ulysses observations of a recurrent high speed solar wind stream and the heliomagnetic streamer belt, *Geophys. Res. Lett.*, *20*(21), 2323.

Birn, J., M. Hesse, and K. Schindler (2006), Entropy conservation in simulations of magnetic reconnection, *Phys. Plasmas*, *13*, 092117.

Borovsky, J. E., and M. H. Denton (2006), Differences between CME-driven storms and CIR-driven storms, *J. Geophys. Res.*, *111*, A07S08, doi:10.1029/2005JA011447.

Borovsky, J. E., M. F. Thomsen, and R. C. Elphic (1998), The driving of the plasma sheet by the solar wind, *J. Geophys. Res.*, *103*(A8), 17,617.

Burton, R. K., R. L. McPherron, and C. T. Russell (1975), An empirical relationship between interplanetary conditions and *Dst*, *J. Geophys. Res.*, *80*(31), 4204.

Denton, M. H., M. F. Thomsen, H. Korth, S. Lynch, J. C. Zhang, and M. W. Liemohn (2005), Bulk plasma properties at geosynchronous orbit, *J. Geophys. Res.*, *110*, A07223, doi:10.1029/2004JA010861.

Denton, M. H., J. E. Borovsky, R. M. Skoug, M. F. Thomsen, B. Lavraud, M. G. Henderson, R. L. McPherron, J. C. Zhang, and M. W. Liemohn (2006), Geomagnetic storms driven by ICME- and CIR-dominated solar wind, *J. Geophys. Res.*, *111*, A07S07, doi:10.1029/2005JA011436.

Elphic, R. C., L. A. Weiss, M. F. Thomsen, D. J. McComas, and M. B. Moldwin (1996), Evolution of plasmaspheric ions at geosynchronous orbit during times of high geomagnetic activity, *Geophys. Res. Lett.*, *23*(16), 2189.

Feynman, J. (1980), Implications of solar cycles 19 and 20 geomagnetic activity for magnetospheric processes, *Geophys. Res. Lett.*, *7*(11), 971.

Friedel, R. H. W., H. Korth, M. G. Henderson, M. F. Thomsen, and J. D. Scudder (2001), Plasma sheet access to the inner magnetosphere, *J. Geophys. Res.*, *106*(A4), 5845.

Gonzalez, W. D., and B. T. Tsurutani (1987), Criteria of interplanetary parameters causing intense magnetic storms (Dst < −100 nT), *Planet. Space Sci.*, *35*, 1101.

Gonzalez, W. D., J. A. Joselyn, Y. Kamide, H. W. Kroehl, G. Rostoker, B. T. Tsurutani, and V. M. Vasyliunas (1994), What is a geomagnetic storm?, *J. Geophys. Res.*, *99*(A4), 5771.

Gosling, J. T., D. J. McComas, J. L. Phillips, and S. J. Bame (1991), Geomagnetic activity associated with Earth passage of interplanetary shock disturbances and coronal mass ejections, *J. Geophys. Res.*, *96*(A5), 7831.

Huttunen, K. E. J., and H. E. J. Koskinen (2004), Importance of post-shock streams and sheath region as drivers of intense magnetospheric storms and high-latitude activity, *Ann. Geophys.*, *22*, 1729.

Huttunen, K. E. J., H. E. J. Koskinen, A. Karinen, and K. Mursula (2006), Asymmetric development of magnetospheric storms during magnetic clouds and sheath regions, *Geophys. Res. Lett.*, *33*, L06107, doi:10.1029/2005GL024894.

Korth, H., M. F. Thomsen, J. E. Borovsky, and D. J. McComas (1999), Plasma sheet access to geosynchronous orbit, *J. Geophys. Res.*, *104*(A11), 25,047.

Kozyra, J. U., V. K. Jordanova, J. E. Borovsky, M. F. Thomsen, D. J. Knipp, D. S. Evans, D. J. McComas, and T. E. Cayton (1998), Effects of a high-density plasma sheet on ring current development during the November 2–6, 1993, magnetic storm, *J. Geophys. Res.*, *103*(A11), 26,285.

Liemohn, M. W., and P. C. Brandt (2005), Small-scale structure in the stormtime ring current, in *Inner Magnetosphere Interactions: New Perspectives From Imaging*, *Geophys. Monogr. Ser.*, vol. 159, edited by J. L. Burch, M. Schulz, and H. Spence, p. 167, AGU, Washington, D. C.

Liemohn, M. W., J. U. Kozyra, V. K. Jordanova, G. V. Khazanov, M. F. Thomsen, and T. E. Cayton (1999), Analysis of early phase ring current recovery mechanisms during geomagnetic storms, *Geophys. Res. Lett.*, *26*(18), 2845.

Liemohn, M. W., J.-C. Zhang, M. F. Thomsen, J. E. Borovsky, J. U. Kozyra, and R. Ilie (2008), Plasma properties of superstorms at geosynchronous orbit: How different are they?, *Geophys. Res. Lett.*, *35*, L06S06, doi:10.1029/2007GL031717.

McComas, D. J., S. J. Bame, B. L. Barraclough, J. R. Donart, R. C. Elphic, J. T. Gosling, M. B. Moldwin, K. R. Moore, and M. F. Thomsen (1993), Magnetospheric plasma analyzer: Initial three-spacecraft observations from geosynchronous orbit, *J. Geophys. Res.*, *98*(A8), 13,453.

O'Brien, T. P., and R. L. McPherron (2000), An empirical phase space analysis of ring current dynamics: Solar wind control of injection and decay, *J. Geophys. Res.*, *105*(A4), 7707.

Pulkkinen, T. I., N. Partamies, K. E. J. Huttunen, G. D. Reeves, and H. E. J. Koskinen (2007), Differences in geomagnetic storms driven by magnetic clouds and ICME sheath regions, *Geophys. Res. Lett.*, *34*, L02105, doi:10.1029/2006GL027775.

Richardson, I. G., E. W. Cliver, and H. V. Cane (2001), Sources of geomagnetic storms for solar minimum and maximum conditions during 1972–2000, *Geophys. Res. Lett.*, *28*(13), 2569.

Thomsen, M. F. (2004), Why *Kp* is such a good measure of magnetospheric convection, *Space Weather*, *2*, S11004, doi:10.1029/2004SW000089.

Thomsen, M. F., J. E. Borovsky, D. J. McComas, and M. R. Collier (1998), Variability of the ring current source population, *Geophys. Res. Lett.*, *25*(18), 3481.

Tsurutani, B. T., and W. D. Gonzalez (1997), The interplanetary causes of magnetic storms, in *Magnetic Storms*, *Geophys. Monogr. Ser.*, vol. 98, edited by B. T. Tsurutani et al., p. 77, AGU, Washington, D. C.

Weimer, D. R. (2004), Correction to Predicting interplanetary magnetic field (IMF) propagation delay times using the minimum variance technique, *J. Geophys. Res.*, *109*, A12104, doi:10.1029/2004JA010691.

Weimer, D. R., D. M. Ober, N. C. Maynard, M. R. Collier, D. J. McComas, N. F. Ness, C. W. Smith, and J. Watermann (2003), Predicting interplanetary magnetic field (IMF) propagation delay times using the minimum variance technique, *J. Geophys. Res.*, *108*(A1), 1026, doi:10.1029/2002JA009405.

Young, D. T., H. Balsiger, and J. Geiss (1982), Correlations of magnetospheric ion composition with geomagnetic and solar activity, *J. Geophys. Res.*, *87*(A11), 9077.

Zhang, J., M. W. Liemohn, J. U. Kozyra, M. F. Thomsen, H. A. Elliott, and J. M. Weygand (2006a), A statistical comparison of solar wind sources of moderate and intense geomagnetic storms at solar minimum and maximum, *J. Geophys. Res.*, *111*, A01104, doi:10.1029/2005JA011065.

Zhang, J., M. W. Liemohn, M. F. Thomsen, J. U. Kozyra, M. H. Denton, and J. E. Borovsky (2006b), A statistical comparison of hot-ion properties at geosynchronous orbit during intense and moderate geomagnetic storms at solar maximum and minimum, *J. Geophys. Res.*, *111*, A07206, doi:10.1029/2005JA011559.

Zhang, J., et al. (2007), Solar and interplanetary sources of major geomagnetic storms (Dst ≤ −100 nT) during 1996–2005, *J. Geophys. Res.*, *112*, A10102, doi:10.1029/2007JA012321.

J. E. Borovsky and M. F. Thomsen, Los Alamos National Laboratory, Los Alamos, NM 87545, USA.

R. Ilie and M. W. Liemohn, Department of Atmospheric, Oceanic and Space Sciences, University of Michigan, Ann Arbor, MI 48109-2143, USA. (rilie@umich.edu)

J. Zhang, Physics and Astronomy Department, Rice University, Houston, TX 77005, USA.